Int. J. Advanced Design and Manufacturing Technology, 2023, Vol. 16, No. 1, pp. 13-27

DOI: 10.30495/ADMT.2022.1951472.1338 ISSN: 2252-0406 https://admt.isfahan.iau.ir

Vibration Analysis of an Imperfect Single-Layer Graphene Sheet using Quasi-3d Theory and Isogeometric Approach

Heidar Fazeli[1], Armen Adamian[2,] *, Ahmad Hosseini-Sianaki[3]

Department of Mechanical Engineering, Central Tehran Branch, Islamic Azad University, Tehran, Iran
E-mail: hei.fazeli.eng@iauctb.ac.ir, arm.adamian@iauctb.ac.ir, a_h_sianaki@iauctb.ac.ir
*Corresponding author

Received: 1 February 2022, Revised: 25 April 2022, Accepted: 30 April 2022

Abstract: In this study, the size-dependent free vibration analysis of a geometrically imperfect single-layer graphene sheet (SLGS) is studied by an isogeometric approach along with the quasi-3D shear and normal deformation theory. Initial geometric imperfections alter the natural frequencies of the graphene sheets that may exist inherently or purposely created by researchers. The initial curvature is modelled by an analytical function in the governing Equations of the plate. A 4-variable quasi-3D theory with a seventh-order distribution function is used to include both shear deformation and thickness stretching influences. A weak form of a nonlocal plate for free vibration analysis is derived that requires the first-order continuity of the displacement fields. Inherent high-order continuity of non-uniform rational B-spline (NURBS) basis functions in isogeometric analysis can meet this condition. A comparison between the present study and other published works reveals the efficiency and accuracy of the proposed method in imperfect SLGS. The results of the present study show a significant effect of initial geometric imperfection on the natural frequency of single-layer graphene sheets.

Keywords: Fundamental Frequency, Imperfection Sensitivity, Initial Geometric Imperfection, Isogeometric Analysis, Single-Layer Graphene

Biographical notes: Heidar Fazeli is a Ph.D. student of mechanical engineering at Central Tehran Branch, IAU, Tehran, Iran. He received his MSc in Mechanical Engineering from Iran University of Science and technology in 2011. **Armen Adamian** is an assistant professor of Mechanical Engineering at the Central Tehran Branch, IAU. He received his Ph.D. in Mechanical Engineering from University of California Los Angeles in 1986. His current research focuses on modal analysis, nanocomposites, structural dynamics. **Ahmad Hosseini-Sianaki** is an assistant professor of Mechanical Engineering at Central Tehran Branch, IAU. He received his Ph.D. in Mechanical engineering from the University of Sussex, England in 1990. His current research focuses on vibration systems and applications of smart materials in engineering and biomechanics.

Research paper

1 INTRODUCTION

In recent years, the invaluable mechanical, electrical, chemical, and thermal properties of nanostructures have encouraged researchers to study and use them in various engineering fields such as biomedical, nanocomposite, and micro/nano-electromechanical systems (MEMS/NEMS) [1].

Single-layer graphene sheet (SLGS) is a carbon-based nanostructure that has become a useful material in sensitive sensors such as nano-resonators, mass sensors, and strain sensors due to its unique properties such as high resonance frequencies and high elastic modulus, [2]. The geometric configuration for the graphene sheet has an essential effect on the mentioned properties that deformation can change them [3]. The pristine graphene sheet can be considered as a flat plate where the carbon atoms are inside a perfect hexagonal lattice. But different defects may appear in these sheets due to the production process. Based on how a defect is formed, it can be classified into three groups: adding carbon or other atoms (adatoms), eliminating carbon atoms from the graphene structure (vacancies) and rearrangement of carbon atoms (such as stone-wales) [4]. With the defects mentioned above, the graphene sheet remains 2D, however researchers [5] have shown that in the presence of some other defects, "graphene reshapes to a 3D state to minimize its energy". This out-of-plane defect is called the initial geometric imperfection [4]. Although the last defect may inevitably occur in a sheet, researchers have recently been able to determine the type and position of defects using manipulated processes to achieve desirable engineered defective graphene sheets [6-7]. Since the imperfection can change the mechanical properties of graphene sheets, understanding the behaviour of the imperfect graphene sheet will help to have an optimal design.

Suleimani et al. [8] analyzed the post-buckling behavior of an SLGS that has an initial geometric imperfection. Jomezadeh et al. [9] investigated the effects of initial configuration for graphene on bending stiffness by extracting non-local Equations for a single-layered graphene sheet with initial curvature. Jalali et al. [4] studied the effect of initial geometric imperfection on graphene sheet vibrations using molecular dynamics and a continuum approach. They observed that the out-of-plane defects increased the natural frequencies of graphene sheets. Implementing precise and controlled experiments at nanoscale is very costly, so researchers have turned to numerical simulations and theoretical analysis to find mechanical properties of nanostructures. There are three approaches available to researchers to implement numerical analysis: molecular dynamics (MD) simulation, continuum methods and combined continuum and molecular dynamics methods. Since molecular dynamics simulation is time-consuming, continuum methods have grown significantly in recent years. When the specimen size is of the order of internal length scale of the material, classical continuum theories are no longer appropriate and the use of nonlocal theories is essential [9]. Eringen's nonlocal elasticity theory [10] is one of the most popular continuum theories known, in which the stress at any point in the body, besides the strain at that point, depends on the strain in all the neighbouring regions in the continuum environment. The nonlocal theory considers inter-atomic forces and applies the internal length scale to the stress-strain Equations [11]. This theory can analyse the behaviour of large Nano-scale structures without having to solve a large number of Equations [12]. This theory, when considering the small-scale effects, provides a satisfactory analysis in comparison with the molecular dynamic's method [13]. From the continuum perspective, an SLGS can be considered as a nanoplate, and hence well-known plate theories can be employed to investigate the vibration response. Classical Plate Theory (CLPT) and first-order shear deformation theory are well-known theories in the analysis of small-scale structures that are used for thin and moderately thick plates, respectively [14-15]. Although the FSDT can be used to analyze moderately thick plates, it's always faced with the problem of selecting the shear correction factor and the shear locking phenomenon. To avoid using the shear correction factors and increase accuracy, researchers use various high-order shear deformation theories [16], [11]. Higher-order theories often have many unknown variables. To reduce the number of variables without decreasing the accuracy, Senthilnathan et al. [17] developed a Refined Plate Theory (RPT) using four independent variables. Subsequently, this theory was used in various nanoscale problems. The buckling and free vibration analysis of orthotropic graphene sheets and nanoplates using RPT was examined by Narendar et al. [18]. Also, Shimpi [19] and Malekzadeh and Shojaee [12] examined the vibrations of a nonlocal rectangular plate using the RPT and the DQM approach. Sarrami-Forushani and Azhari [11] studied the buckling and vibrations of thick rectangular graphene nanoplates using RPT and the finite strip method. In the theories mentioned above, the effects of thickness stretching are neglected, while these effects must be considered in the case of 3D strain $(\varepsilon_z \neq 0)$. For this purpose, high-order shear and normal deformation theories named quasi-3D can be used [20]. Zenkour [21] presented a four variables quasi-3D theory for the static analysis of FGM plates. Subsequently, this quasi-3D theory was used to analyze the bending behavior of FGM plates using the Navier approach [22]. Also, in various papers, the vibrations of plates and nanoplates are investigated using polynomial and non-

polynomial high order shear and normal deformation theory [20], [23-25]. In nanoplates modeling using RPT and quasi-3D theories, the displacement field requires at least C^1 continuity, whereas conventional finite element methods have C^0 continuity and cannot be used easily without adding variables [26]. For this purpose, Hughes et al. [27] presented a numerical method combining computer-aided design and Finite Element Analysis (FEA) based on Galerkin's weak form, named isogeometric analysis (IGA). In this method, a non-uniform rational B-spline basis function (NURBS) is used to describe the structure and also the solution field approximation simultaneously. These B-splines can easily meet the requirements of high-order continuity. Subsequently, because of unique features such as accurate geometry representation, and no need for high-level meshing and continuity, the IGA is widely used in analyzing plates and nanoplates with various plate theories such as FSDT [8], RPT, and quasi-3D theory [20-23], [25], [28].

As mentioned in the literature review, no study has been carried out on the nonlocal vibration analysis of SLGS with an initial geometric imperfection using the quasi-3D theory based on the IGA approach. In the present work, a four-variables quasi-3d theory is proposed to represent the displacement Equations of the plate. The initial geometric imperfection is given as a parametric function and two types of imperfections (sinusoidal and L1 types) are investigated. Using Eringen's nonlocal theory, small-scale effects are applied in the stress-strain Equation. A discrete system of Equations is extracted using the Hamilton principle and is solved by the isogeometric method. The effects of the imperfection amplitude, nonlocal parameter, plate geometrical parameters, and boundary conditions on the imperfection sensitivity and natural frequency of SLGS have been investigated. The comparison between present study and other published works indicates the efficiency and accuracy of the proposed method in imperfect SLGS.

2 GOVERNING EQUATIONS

2.1. Higher-Order Plate Theories

A rectangular graphene sheet that in the continuum approach is assumed as a nanoplate with length a, width b, and the uniform thickness h, is depicted in "Fig. 1".

If the thickness to side ratio for the nanoplate is very small, classical and first-order shear deformation theories can be used, but as the thickness increases, these theories are not accurate enough due to the lack of the shear effects consideration. By taking into account the shear effects, higher-order terms appear in the plate displacement field. Soldatos [29], using the generalized higher-order shear deformation theory, showed the displacement field as:

$$\begin{aligned} u(x,y,z) &= u_0(x,y) - zw_{,x}(x,y) + f(z)\beta_x(x,y) \\ v(x,y,z) &= v_0(x,y) - zw_{,y}(x,y) + f(z)\beta_y(x,y) \\ w(x,y) &= w_0(x,y) \end{aligned} \quad (1)$$

Where, u_0, v_0, and w_0 are the mid-plane displacements of the sheet along x, y, and z, and β_x, β_y are rotations about yz and xz plane, respectively. As it can be seen, in this theory, five variables are used.

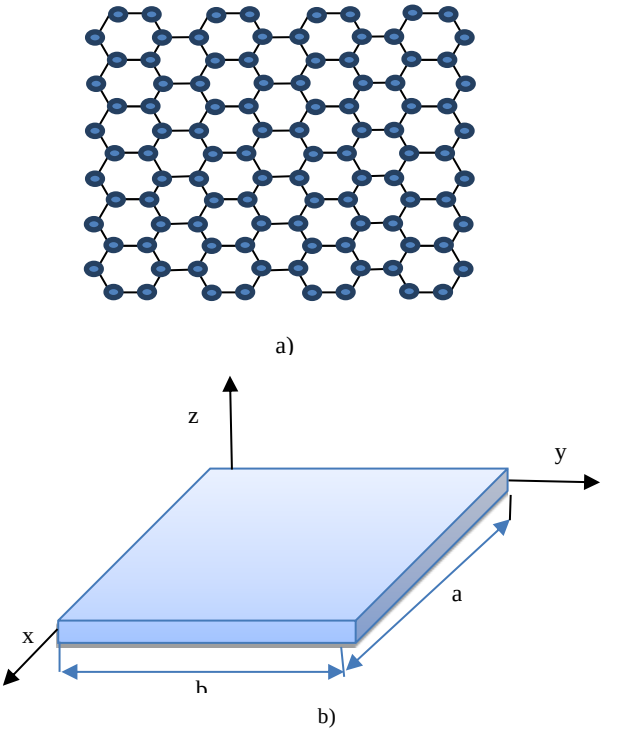

Fig. 1 Single-layer graphene Sheet: (a): Hexagonal lattice, and (b): Continuum model.

Senthilnathan [17] has introduced a refined plate theory (RPT) which uses four unknown variables:

$$\begin{aligned} u(x,y,z) &= u_0(x,y) - zw^b{}_{,x}(x,y) + g(z)w^s{}_{,x}(x,y) \\ v(x,y,z) &= v_0(x,y) - zw^b{}_{,y}(x,y) + g(z)w^s{}_{,y}(x,y) \\ w(x,y) &= w^b(x,y) + w^s(x,y) \end{aligned} \quad (2)$$

Where, w^b and w^s are the bending and shear deformations of the plate in the z-direction, respectively, and $g(z)=f(z)-z$. In the plate theories mentioned above, the effect of thickness stretching in the z-direction is not considered. To overcome this shortcoming, Zenkour

[21] presented a quasi-3D plate theory which has four unknown variables:

$$\begin{aligned} u(x,y,z) &= u_0(x,y) - zw^b{}_{,x}(x,y) + f(z)w^s{}_{,x}(x,y) \\ v(x,y,z) &= v_0(x,y) - zw^b{}_{,y}(x.y) + f(z)w^s{}_{,y}(x,y) \\ w(x,y,z) &= w^b(x,y) + \phi(z)w^s(x,y) \end{aligned} \quad (3)$$

The refined plate theory ("Eq. (2)") can be obtained by replacing $\phi(z)=1$ and *f(z)=g(z)* in "Eq. (3)". Different distribution functions have been used in various papers. In "Table 1", some of these functions are given based on the RPT and quasi-3D theory.

Table 1 Distribution functions used in various papers

Model	ε_z	*f(z)*	*Φ(z)*
Soldatos RPT [29]	*=0*	$h\sinh\left(\frac{z}{h}\right) - z\cosh\left(\frac{1}{2}\right)$	1
Nguyen RPT [30]	*=0*	$\frac{7}{8}z - \frac{2}{h^2}z^3 + \frac{2}{h^4}z^5$	1
Nguyen RPT [31]	*=0*	$\tan^{-1}(\sin(\pi z/h))$	1
Nguyen Quasi-3D [20]	*≠0*	$\frac{\pi}{h}z - \frac{9\pi}{5h^3}z^3 + \frac{28\pi}{25h^5}z^5$	$\frac{1}{8}f'(z)$
Zenkour Quasi-3D [22]	*≠0*	$h\sinh\left(\frac{z}{h}\right) - \frac{4z^3}{3h^2}\cosh\left(\frac{1}{2}\right)$	$\frac{1}{12}f'(z)$
Nguyen Quasi-3D [23]	*≠0*	$-8z + \frac{10}{h^2}z^3 + \frac{6}{5h^4}z^5 + \frac{8}{7h^6}z^7$	$\frac{3}{20}f'(z)$
Thai Quasi-3D [32]	*≠0*	$\frac{h}{\pi}\sin(\frac{\pi z}{h})$	$f'(z)$
Gupta Quasi-3D [35]	*≠0*	$\frac{-h\cosh^2\left(\frac{k}{2}\right)}{\sqrt{(1+\frac{k^2}{4})}-1}(\sinh^{-1}\left(\frac{kz}{h}\right) - \left(\frac{kz}{h}\right))$	$k\cosh^2(kz/h)$

In the presence of the initial geometric imperfection, the plate will become three-dimensional. Assuming that the initial geometric imperfection in the nanoplate exists only in the transverse direction, the displacement Equation can be corrected as follows [4], [8]:

$$\begin{aligned} u(x,y,z) &= u_0(x,y) - zw^b{}_{,x}(x,y) + f(z)w^s{}_{,x}(x,y) \\ v(x,y,z) &= v_0(x,y) - zw^b{}_{,y}(x,y) + f(z)w^s{}_{,y}(x,y) \\ w(x,y,z) &= w^b(x,y) + \phi(z)w^s(x,y) + w^i(x,y) \end{aligned} \quad (4)$$

Where, $w^i(x,y)$ denotes the initial geometric imperfection function in the nanoplate.

2.2. Size-Dependent Plate Theory

By using Eringen's nonlocal elasticity theory, the stress-strain relations are simplified in the following way:

$$\left(1-\mu\nabla^2\right)\sigma_{ij} = C_{ijkl}\varepsilon_{kl} \quad (5)$$

Where, $\mu=(e_0a_0)^2$ is the small-scale parameter (e_0 and a_0 are respectively the material constant, and the internal characteristic length) and ∇^2 is the Laplacian operator. Using "Eq. (5)", nonlocal constitutive Equations for a nonlocal plate can be expressed by:

$$\begin{bmatrix}\sigma_{xx}\\ \sigma_{yy}\\ \sigma_{zz}\\ \sigma_{xy}\\ \tau_{xz}\\ \tau_{yz}\end{bmatrix} - \mu\nabla^2\begin{bmatrix}\sigma_{xx}\\ \sigma_{yy}\\ \sigma_{zz}\\ \sigma_{xy}\\ \tau_{xz}\\ \tau_{yz}\end{bmatrix} = \begin{bmatrix} C_{11} & C_{12} & C_{13} & 0 & 0 & 0 \\ C_{21} & C_{22} & C_{23} & 0 & 0 & 0 \\ C_{31} & C_{32} & C_{33} & 0 & 0 & 0 \\ 0 & 0 & 0 & C_{66} & 0 & 0 \\ 0 & 0 & 0 & 0 & C_{55} & 0 \\ 0 & 0 & 0 & 0 & 0 & C_{44} \end{bmatrix}\begin{bmatrix}\varepsilon_{xx}\\ \varepsilon_{yy}\\ \varepsilon_{zz}\\ \gamma_{xy}\\ \gamma_{xz}\\ \gamma_{yz}\end{bmatrix} \quad (6)$$

If the quasi-3D theory is used, the elastic constants for the state $\varepsilon_z \neq 0$ will be [21]:

$$C_{11}=C_{22}=C_{33}=\frac{E(1-\nu)}{(1-2\nu)(1+\nu)}$$
$$C_{12}=C_{21}=C_{13}=C_{31}=C_{23}=C_{32}=\frac{E\nu}{(1-2\nu)(1+\nu)} \quad (7)$$
$$C_{44}=C_{55}=C_{66}=\frac{E}{2(1+\nu)}$$

However, if the RPT is used, the elastic constants for the plane stress state $(\varepsilon_z=0)$ can be written as:

$$C_{11}=C_{22}=\frac{E}{1-\nu^2}, \qquad C_{12}=C_{21}=\frac{E\nu}{1-\nu^2}$$
$$C_{13}=C_{31}=C_{23}=C_{32}=C_{32}=0 \quad (8)$$
$$C_{44}=C_{55}=C_{66}=\frac{E}{2(1+\nu)}$$

Using "Eq. (4)", the Von Karman [22] strain-displacement relationship at a chosen point on the sheet can be described as:

$$\varepsilon = \begin{bmatrix}\varepsilon_{xx}\\ \varepsilon_{yy}\\ \gamma_{xy}\end{bmatrix} = \varepsilon_0 + z\varepsilon_1 + f(z)\varepsilon_2 + \Phi(z)\varepsilon_3$$
$$\gamma = \begin{bmatrix}\gamma_{xz}\\ \gamma_{yz}\end{bmatrix} = \left[f'(z)+\Phi(z)\right]\varepsilon_s, \varepsilon_z = \Phi'(z)w^s \quad (9)$$

Where:

$$\varepsilon_0 = \begin{bmatrix} u_{0,x}+w^b{}_{,x}w^i{}_{,x} \\ v_{0,y}+w^b{}_{,y}w^i{}_{,y} \\ u_{0,y}+v_{0,x}+w^b{}_{,x}w^i{}_{,y}+w^b{}_{,y}w^i{}_{,x}\end{bmatrix},$$
$$\varepsilon_1 = -\begin{bmatrix} w^b{}_{,xx} \\ w^b{}_{,yy} \\ 2w^b{}_{,xy}\end{bmatrix}, \varepsilon_2 = \begin{bmatrix} w^s{}_{,xx} \\ w^s{}_{,yy} \\ 2w^s{}_{,xy}\end{bmatrix}, \quad (10)$$
$$\varepsilon_3 = \begin{bmatrix} w^s{}_{,x}w^i{}_{,x} \\ w^s{}_{,y}w^i{}_{,y} \\ w^s{}_{,x}w^i{}_{,y}+w^s{}_{,y}w^i{}_{,x}\end{bmatrix}, \ \varepsilon_s = \begin{bmatrix} w^s{}_{,x} \\ w^s{}_{,y}\end{bmatrix}$$

The stress resultants can be considered as:

$$(N_{ij}, M^b{}_{ij}, M^s{}_{ij}, M^i{}_{ij}) = \int_{-\frac{h}{2}}^{\frac{h}{2}} \sigma_{ij}\left(1, z, f(z), \Phi(z)\right)dz \ , ij = xx, yy, xy$$

$$R_z = \int_{-\frac{h}{2}}^{\frac{h}{2}} \sigma_{zz}\Phi'(z)dz \quad (11)$$
$$Q_{ij} = \int_{-\frac{h}{2}}^{\frac{h}{2}} \tau_{ij}\left(f'(z)+\Phi(z)\right)dz \quad , ij = xz, yz$$

Now using Eqs. (9) to (11), Eq. (6) can be rewritten as stress resultants:

$$\begin{bmatrix} N \\ M^b \\ M^s \\ M^i \\ R_z\end{bmatrix} - \mu\nabla^2 \begin{bmatrix} N \\ M^b \\ M^s \\ M^i \\ R_z\end{bmatrix} = D^b\varepsilon^b, \quad Q-\mu\nabla^2 Q = D^s\varepsilon^s \quad (12)$$

Where the material matrices are:

$$D^b = \begin{bmatrix} A & B & E & K & X \\ & D & F & L & Y^b \\ & & H & O & Y^s \\ & & & P^1 & Y^i \\ sym & & & & Z_{33}\end{bmatrix}$$
$$(A_{ij}, B_{ij}, D_{ij}, E_{ij}, F_{ij}, H_{ij}, K_{ij}, L_{ij}, O_{ij}, P_{ij}) =$$
$$\int_{-\frac{h}{2}}^{\frac{h}{2}} \begin{pmatrix} 1, z, z^2, f(z), zf(z), \left(f(z)\right)^2 \\ , \Phi(z), z\Phi(z), f(z)\Phi(z), \left(\Phi(z)\right)^2\end{pmatrix} \bar{C}_{ij}dz \quad (13)$$

$$(X_{ij}, Y^b{}_{ij}, Y^s{}_{ij}, Y^i{}_{ij}) =$$
$$\int_{-\frac{h}{2}}^{\frac{h}{2}} (\Phi'(z), z\Phi'(z), f(z)\Phi'(z), \Phi(z)\Phi'(z))\hat{C}_{ij}dz$$

$$Z_{33} = \int_{-\frac{h}{2}}^{\frac{h}{2}} (\Phi'(z))^2 C_{33}dz$$
$$, D^s{}_{ij} = \int_{-\frac{h}{2}}^{\frac{h}{2}} \left(f'(z)+\Phi(z)\right)^2 \tilde{C}_{ij}dz \quad (14)$$

In which:

$$\bar{C}_{ij}=\begin{bmatrix} C_{11} & C_{12} & 0 \\ & C_{22} & 0 \\ sym & & C_{66} \end{bmatrix},\qquad \hat{C}_{ij}=\begin{bmatrix} C_{13} \\ C_{23} \\ 0 \end{bmatrix},$$
$$\tilde{C}_{ij}=\begin{bmatrix} C_{55} & 0 \\ 0 & C_{44} \end{bmatrix} \tag{15}$$

And also, the strain tensor ε^b is:

$$\varepsilon^b=\begin{bmatrix} \varepsilon_0 \\ \varepsilon_1 \\ \varepsilon_2 \\ \varepsilon_3 \\ w^s \end{bmatrix} \tag{16}$$

To derive the governing Equations of the graphene sheet, Hamilton's principle is expressed as:

$$\int_0^t \left(\delta U+\delta V-\delta T\right)dt=0 \tag{17}$$

The variation of strain energy can be expressed by:

$$\delta U=\int_V(\sigma^T\delta\varepsilon)dV=\iint_A\int_{-\frac{h}{2}}^{\frac{h}{2}}\left(\begin{bmatrix}\sigma_{xx}\\ \sigma_{yy}\\ \sigma_{xy}\end{bmatrix}^T\delta\left(\begin{bmatrix}\varepsilon_{xx}\\ \varepsilon_{yy}\\ \gamma_{xy}\end{bmatrix}\right)\right.$$
$$\left.+\begin{bmatrix}\tau_{xz}\\ \tau_{yz}\end{bmatrix}^T\delta\left(\begin{bmatrix}\gamma_{xz}\\ \gamma_{yz}\end{bmatrix}\right)+{\sigma_{zz}}^T\delta\varepsilon_z\right)dzdA=$$
$$\int_A\left(N_{xx}\left(\delta u_{0,x}+w^i{}_{,x}\delta w^b{}_{,x}\right)+N_{yy}\left(\delta v_{0,y}+w^i{}_{,y}\delta w^b{}_{,y}\right)\right.$$
$$+N_{xy}\left(\delta u_{0,y}+\delta v_{0,x}+w^i{}_{,y}\delta w^b{}_{,x}+w^i{}_{,x}\delta w^b{}_{,y}\right)+$$
$$M^b{}_{xx}\left(-\delta w^b{}_{,xx}\right)+M^b{}_{yy}\left(-\delta w^b{}_{,yy}\right)+M^b{}_{xy}\left(-2\delta w^b{}_{,x}\right) \tag{18}$$
$$+M^s{}_{xx}\left(\delta w^s{}_{,xx}\right)+M^s{}_{yy}\left(\delta w^s{}_{,yy}\right)+M^s{}_{xy}\left(2\delta w^s{}_{,xy}\right)+$$
$$M^i{}_{xx}\left(w^i{}_{,x}\delta w^s{}_{,x}\right)+M^i{}_{yy}\left(w^i{}_{,y}\delta w^s{}_{,y}\right)+$$
$$M^i{}_{xy}\left(w^i{}_{,y}\delta w^s{}_{,x}+w^i{}_{,x}\delta w^s{}_{,y}\right)+Q_{xz}\left(\delta w^s{}_{,x}\right)+Q_{yz}\left(\delta w^s{}_{,y}\right)$$
$$\left.+R_z\delta w^s\right)dA$$

Also, the variation of work done by external forces is:

$$\delta V=\int_V(-q\delta w)dV=\int_A\int_{-\frac{h}{2}}^{\frac{h}{2}}q\delta(w^b+\phi(z)w^s+w^i)dzdA \tag{19}$$

Since $\delta w^i=0$ and q=0, therefore:

$$\delta V=-\int_A\int_{-\frac{h}{2}}^{\frac{h}{2}}q(\delta w^b+\phi(z)\delta w^s)dzdA=$$
$$-\int_A q(\delta w^b+\phi(\frac{h}{2})\delta w^s)dA=0 \tag{20}$$

The variation of kinetic energy can also be written as:

$$\delta T=\int_V\rho\dot{\bar{u}}^T\delta\dot{\bar{u}}dV \tag{21}$$

Considering $u=\begin{bmatrix}u_0 & -w^b{}_{,x} & w^s{}_{,x} & v_0 & -w^b{}_{,y} & w^s{}_{,y} & w^b & w^s & 0\end{bmatrix}^T$, the above Equation can be expressed as:

$$\delta T=-\int_A\int_{-\frac{h}{2}}^{\frac{h}{2}}\rho\left(\left(\dot{u}_0-z\dot{w}^b_{,x}+f(z)\dot{w}^s_{,x}\right)\begin{pmatrix}\delta\dot{u}_0-z\delta\dot{w}^b_{,x}\\ +f(z)\delta\dot{w}^s_{,x}\end{pmatrix}\right.$$
$$+\left(\dot{v}_0-z\dot{w}^b_{,y}+f(z)\dot{w}^s_{,y}\right)\left(\delta\dot{v}_0-z\delta\dot{w}^b_{,y}+f(z)\delta\dot{w}^s_{,y}\right) \tag{22}$$
$$\left.+(\dot{w}^b+\phi(z)\dot{w}^s)(\delta\dot{w}^b+\phi(z)\delta\dot{w}^s)\right)dzdA$$

"Eq. (22)" can be simply rewritten as:

$$\delta T=\int_V\ddot{\bar{u}}^T m\delta\dot{\bar{u}}dV \tag{23}$$

In which the mass matrix is defined as:

$$m=\begin{bmatrix}m_0 & 0 & 0\\ 0 & m_0 & 0\\ 0 & 0 & m_1\end{bmatrix},\ m_0=\begin{bmatrix}I_1 & I_2 & I_4\\ I_2 & I_3 & I_5\\ I_4 & I_5 & I_6\end{bmatrix},$$
$$m_1=\begin{bmatrix}I_1 & I_7 & 0\\ I_7 & I_8 & 0\\ 0 & 0 & 0\end{bmatrix} \tag{24}$$

$$I_1,I_2,I_3,I_4,I_5,I_6,I_7,I_8=$$
$$\int_{-\frac{h}{2}}^{\frac{h}{2}}\rho(1,z,z^2,f(z),zf(z),\left(f(z)\right)^2,\Phi(z),\left(\Phi(z)\right)^2)dz \tag{25}$$

The governing Equations for the plate in the displacement form can be obtained by inserting "Eqs. (18), (20), and (23)" in "Eq. (17)", and then integrating by parts and sorting gives:

$$
\begin{aligned}
&\delta u_0: \quad N_{xx,x}+N_{xy,y}=I_1\ddot{u}_0-I_2\ddot{w}^b_{,x}+I_4\ddot{w}^s_{,x}\\
&\delta v_0: \quad N_{yy,y}+N_{xy,x}=I_1\ddot{v}_0-I_2\ddot{w}^b_{,y}+I_4\ddot{w}^s_{,y}\\
&\delta w^b:(N_{xx}w^i{}_{,x})_{,x}+(N_{yy}w^i{}_{,y})_{,y}+(N_{xy}w^i{}_{,y})_{,x}\\
&+(N_{xy}w^i{}_{,x})_{,y}+M^b{}_{xx,xx}+M^b{}_{yy,yy}-2M^b{}_{xy,xy}=\\
&I_1\ddot{w}^b+I_2\left(\ddot{u}_{0,x}+\ddot{v}_{0,y}\right)-I_3\left(\ddot{w}^b_{,xx}+\ddot{w}^b_{,yy}\right)+\\
&I_5\left(\ddot{w}^s_{,xx}+\ddot{w}^s_{,yy}\right)+I_7\ddot{w}^s\\
&\delta w^s: \; -M^s{}_{xx,xx}-M^s{}_{yy,yy}-2M^s{}_{xy,xy}-R_z+Q_{xz,x}\\
&+Q_{yz,y}+(M^i{}_{xx}w^i{}_{,x})_{,x}+(M^i{}_{yy}w^i{}_{,y})_{,y}+(M^i{}_{xy}w^i{}_{,x})_{,y}\\
&+(M^i{}_{xy}w^i{}_{,y})_{,x}=-I_4\left(\ddot{u}_{0,x}+\ddot{v}_{0,y}\right)+I_5\left(\ddot{w}^b_{,xx}+\ddot{w}^b_{,yy}\right)\\
&-I_6\left(\ddot{w}^s_{,xx}+\ddot{w}^s_{,yy}\right)+I_7\ddot{w}^b+I_8\ddot{w}^s
\end{aligned}
\tag{26}
$$

After inserting "Eqs (10) to (15)" in "Eq. (26)", the above Equations must be pre-multiplied by $\delta u_0, \delta v_0, \delta w^b, \delta w^s$, respectively and integrated by part in a region to extract the nonlocal weak form. Readers can refer to [20] for further explanation. The nonlocal weak form for the free vibration problem is summarized in the following:

$$
\begin{aligned}
&\int_A((\delta\varepsilon^b)^T D^b\varepsilon^b dA+\int_A((\delta\varepsilon^s)^T D^s\varepsilon^s dA+\\
&\int_A(\delta u^T-\mu\nabla^2\delta u^T)m\ddot{u}\,dA
\end{aligned}
\tag{27}
$$

As it can be seen from "Eq. (27)", the plate transverse deflection variables (w^b, w^s) appear in the form of third-order derivatives due to the nonlocal effects and are accompanied by the Laplacian operator. So, the interpolation functions in the conventional finite element method must have at least a third-degree derivative and satisfy the C^1 continuity, which cannot easily be accomplished. Therefore, the isogeometric approach along with NURBS basis functions can be used well to solve nonlocal SLGS Equations using RPT and quasi-3D theory.

3 IGA FOR FREE VIBRATION PROBLEM

3.1. Summary of NURBS Basis Functions

The NURBS basis functions are applied in both modeling geometries and finite element analysis in IGA. In one dimensional parametric space $(\xi\in[0,1])$, NURBS basis functions are composed of a set of non-decreasing real numbers $K(\xi)=\{\xi1=0,\xi2,\ldots,\xi_i,\ldots,\xi_{n+p+1}=1\}$, that are called knot vectors (ξ_i, p, n are knots, the polynomial order, and the number of basis functions, respectively), and a set of control points.

Each B-spline has a C^∞ continuity inside the knot space and a C^{p-1}continuity at a single knot. The continuity at a knot where repeats k times, is C^{p-k}. The i'th B-spline basis function is written as the following recursive form [23]:

$$
\begin{aligned}
&N_{i,0}(\xi)=\begin{cases}1 & if\ \ \xi_i\le\xi\le\xi_{i+1}\\ 0 & else\end{cases} \qquad \text{for } p=0\\
&N_{i,p}(\xi)=\frac{\xi-\xi_i}{\xi_{i+p}-\xi_i}N_{i,p-1}(\xi)+\frac{\xi_{i+p+1}-\xi}{\xi_{i+p+1}-\xi_{i+1}}N_{i+1,p-1}(\xi)\\
&\text{for } p\ge1
\end{aligned}
\tag{28}
$$

The two-dimensional basis functions are obtained by the tensor product of two one-dimensional B-spline basis functions as:

$$
N_I(\xi,\eta)=N_{i,p}(\xi)N_{j,q}(\eta) \tag{29}
$$

Where, $N_{i,p}(\xi)$ and $N_{j,q}(\eta)$ are the B-spline basis functions with an order of p in the ξ direction and order of q in the η direction, respectively. Fig. 2 shows the B-spline basis functions.

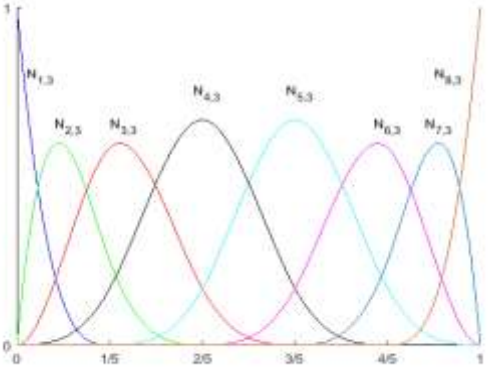

Fig. 2 Cubic basis functions for open non-uniform knot vector $\xi=\{0,0,0,0,\frac{1}{5},\frac{2}{5},\frac{3}{5},\frac{4}{5},1,1,1,1\}$.

B-spline basis functions cannot accurately represent cone shapes like circles and ellipses. Using NURBS, these shapes can be displayed accurately. Two dimensional NURBS basis function for a NURBS surface can be derived from the following Equation:

$$
R_I(\xi,\eta)=\frac{N_I(\xi,\eta)W_I}{\sum_{I=1}^{m\times n}(N_I(\xi,\eta)W_I)} \tag{30}
$$

In which W_I shows the two-dimensional weight function.

3.2. Quasi-3D Nanoplate Formulation Based on NURBS Basis Function

The displacement variables using NURBS basis functions can be interpolated as follows:

$$u^h(\xi,\eta)=\sum_{I=1}^{m\times n}\left(R_I(\xi,\eta)u_I\right) \tag{31}$$

Where, $u_I=\begin{bmatrix}u_0 & v_0 & w^b & w^s\end{bmatrix}$ is the degrees of freedom vector associated with the control point I, and $m \times n$ is the number of basis functions. Using "Eq. (31)", the in-plane, normal and shear strains "Eq. (10)" can be rewritten as:

$$\varepsilon_0=\sum_{I=1}^{m\times n}\left(\begin{bmatrix}R_{I,x} & 0 & R_{I,x}w^i{}_{,x} & 0\\ 0 & R_{I,y} & R_{I,y}w^i{}_{,y} & 0\\ R_{I,y} & R_{I,x} & R_{I,x}w^i{}_{,y}+R_{I,y}w^i{}_{,x} & 0\end{bmatrix}\begin{Bmatrix}u_{0I}\\ v_{0I}\\ w^b{}_I\\ w^s{}_I\end{Bmatrix}\right)=$$

$$\sum_{I=1}^{m\times n}B^m{}_Iu_I$$

$$\varepsilon_1=\sum_{I=1}^{m\times n}\left(-\begin{bmatrix}0 & 0 & R_{I,xx} & 0\\ 0 & 0 & R_{I,yy} & 0\\ 0 & 0 & 2R_{I,xy} & 0\end{bmatrix}\begin{Bmatrix}u_{0I}\\ v_{0I}\\ w^b{}_I\\ w^s{}_I\end{Bmatrix}\right)=\sum_{I=1}^{m\times n}B^1{}_Iu_I$$

$$\varepsilon_2=\sum_{I=1}^{m\times n}\left(\begin{bmatrix}0 & 0 & 0 & R_{I,xx}\\ 0 & 0 & 0 & R_{I,yy}\\ 0 & 0 & 0 & 2R_{I,xy}\end{bmatrix}\begin{Bmatrix}u_{0I}\\ v_{0I}\\ w^b{}_I\\ w^s{}_I\end{Bmatrix}\right)=\sum_{I=1}^{m\times n}B^2{}_Iu_I$$

$$\varepsilon_3=\sum_{I=1}^{m\times n}\left(\begin{bmatrix}0 & 0 & 0 & R_{I,x}w^i{}_{,x}\\ 0 & 0 & 0 & R_{I,y}w^i{}_{,y}\\ 0 & 0 & 0 & R_{I,x}w^i{}_{,y}+R_{I,y}w^i{}_{,x}\end{bmatrix}\begin{Bmatrix}u_{0I}\\ v_{0I}\\ w^b{}_I\\ w^s{}_I\end{Bmatrix}\right)$$

$$=\sum_{I=1}^{m\times n}B^3{}_Iu_I$$

$$\varepsilon^s=\sum_{I=1}^{m\times n}\left(\begin{bmatrix}0 & 0 & 0 & R_{I,x}\\ 0 & 0 & 0 & R_{I,y}\end{bmatrix}\begin{Bmatrix}u_{0I}\\ v_{0I}\\ w^b{}_I\\ w^s{}_I\end{Bmatrix}\right)=\sum_{I=1}^{m\times n}B^s{}_Iu_I \tag{32}$$

Also, according to "Eq. (9)", we can write:

$$\varepsilon_z=\sum_{I=1}^{m\times n}\left(\begin{bmatrix}0 & 0 & 0 & R_I\end{bmatrix}\begin{Bmatrix}u_{0I}\\ v_{0I}\\ w^b{}_I\\ w^s{}_I\end{Bmatrix}\right)=\sum_{I=1}^{m\times n}B^z{}_Iu_I \tag{33}$$

The free vibration Equations in matrix form can be obtained by inserting "Eqs. (32), (33)" in "Eq. (27)":

$$\left(\left[K\right]+\omega^2\left[M\right]\right)u=0 \tag{34}$$

In which the general stiffness and mass matrices are:

$$K=\int_A\left(\begin{bmatrix}B^m\\ B^1\\ B^2\\ B^3\\ B^z\end{bmatrix}^T\boldsymbol{D^b}\begin{bmatrix}B^m\\ B^1\\ B^2\\ B^3\\ B^z\end{bmatrix}+\left(B^s\right)^T\boldsymbol{D^s}B^s\right)dA$$

$$M=\int_A\left(\left(\begin{bmatrix}R_1\\ R_2\\ R_3\end{bmatrix}^T-\mu\nabla^2\begin{bmatrix}R_1\\ R_2\\ R_3\end{bmatrix}^T\right)\boldsymbol{m}\begin{bmatrix}R_1\\ R_2\\ R_3\end{bmatrix}\right)dA \tag{35}$$

Where:

$$R_1=\begin{bmatrix}R_I & 0 & 0 & 0\\ 0 & 0 & -R_{I,x} & 0\\ 0 & 0 & 0 & R_{I,x}\end{bmatrix},\ R_2=\begin{bmatrix}0 & R_I & 0 & 0\\ 0 & 0 & -R_{I,y} & 0\\ 0 & 0 & 0 & R_{I,y}\end{bmatrix}$$

$$,\ R_3=\begin{bmatrix}0 & 0 & R_I & R_I\\ 0 & 0 & 0 & 0\\ 0 & 0 & 0 & 0\end{bmatrix} \tag{36}$$

4 NUMERICAL RESULTS AND DISCUSSION

In this section, the vibration behavior of a geometrically imperfect graphene sheet has been investigated. Numerical integrations have been implemented using 4×4 Gaussian quadrature points with cubic NURBS elements. A seventh-order polynomial distribution function f(z) is chosen to satisfy the zero-traction boundary conditions at the top and bottom surfaces of the plate. Therefore, there is no need to select the shear correction factor. The coefficients are obtained by performing the optimization method in such a way that the difference between present results and results from other researchers are minimized.

$$f(z)=\frac{11z}{8}-\frac{11z^3}{6h^2}+\frac{7z^5}{20h^4}-\frac{z^7}{h^6}$$
$$\phi(z)=\frac{1}{3}f'(z) \quad (37)$$

The boundary conditions on the edges of the plate are considered as:

Simply supported (S):

$$v_0=w^b=w^s=0 \qquad at \quad x=0,a$$
$$u_0=w^b=w^s=0 \qquad at \quad y=0,b \quad (38)$$

Clamped (C):

$$u_0=v_0=w^b=w^s=0$$
$$w^b{}_{,x}=w^b{}_{,y}=w^s{}_{,x}=w^s{}_{,y}=0 \quad \text{at all edges} \quad (39)$$

The Dirichlet boundary conditions can easily be applied in the same way as traditional FEM. For normal slopes e.g., $w^b{}_{,x}$, $w^b{}_{,y}, w^s{}_{,x}$ and $w^s{}_{,y}$, Auricchio et al. [33] presented a simple and appropriate solution. In addition to displacements at the boundary control points, they imposed zero values for transverse bending and shear displacements adjacent to the boundary control points.
To investigate the convergence, a pristine square SLGS with Young modulus E=1.06 TPa, thickness h=0.34 nm, density ρ= $2250\frac{kg}{m^3}$, and a width of a=10 nm is used. Both localized (μ=0) and nonlocalized (μ=1) assumptions, and simply supported boundary conditions (SSSS) are implemented. The fundamental frequencies for several elements are given in "Table 2". To carry out the best comparison with existing papers, a refined plate theory is used.

Table 2 Convergence of fundamental frequency (THZ) for pristine SLGS (a=10, v=0.25)

		$\mu=0$	$\mu=1$
Element Mesh	7×7	0.068915	0.062979
	9×9	0.068914	0.062978
	11×11	0.068913	0.062978
	13×13	0.068913	0.062978
	RPT [11]	0.068917	0.062981
	CPT [34]	0.069126	0.063172

As it can be seen, responses converge after applying 11 grid points. Therefore, in continuing this study, a mesh of 11×11 cubic NURBS elements is used in the numerical calculations. This mesh and the corresponding control points are shown in "Fig. 3".

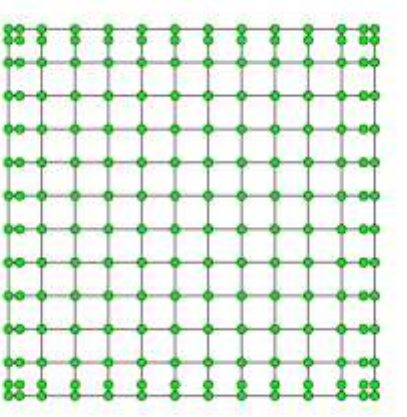

Fig. 3 Control point net and element mesh for SLGS.

To verify the present results, first a nonlocal pristine graphene sheet (without geometric imperfection) and then a localized imperfect graphene sheet are analyzed, and the results are compared with published papers. A pristine graphene sheet with the specifications mentioned before and a length of 5 nm and 10 nm are considered. Simply supported boundary condition is applied, and results for different aspect ratios and nonlocal parameters are shown in "Table 3".

Table 3 Fundamental frequencies (THZ) of SSSS pristine SLGS(v=0.25)

μ	a	$\frac{b}{a}$	Present RPT	Present quasi-3D	RPT [11]	CPT [34]
0	5	1	0.273212	0.278897	0.273201	0.276505
		2	0.171514	0.175296	0.171533	0.172833
		3	0.152583	0.155983	0.152608	0.153636
	10	1	0.068913	0.070522	0.068917	0.069126
		2	0.043120	0.044140	0.043126	0.043208
		3	0.038337	0.039246	0.038344	0.038409
1	5	1	0.204233	0.208482	0.204224	0.206694
		2	0.140346	0.143441	0.140361	0.141425
		3	0.127212	0.130047	0.127233	0.128090
	10	1	0.062978	0.064447	0.062981	0.063172
		2	0.040683	0.041646	0.040689	0.040767
		3	0.036393	0.037256	0.036400	0.036462

The fundamental frequencies obtained using present RPT and quasi-3D methods are compared with the results from other researchers. Results are in good agreement with the RPT [11] and CPT [34]. Due to stretching effects, Quasi-3D theory gives larger responses than RPT and CPT. For thinner sheets (a = 10), frequencies for different plate theories are very close to each other, while in thicker sheets (a = 5), they are somewhat different. As the nonlocal parameter increases, the fundamental frequency decreases due to a decrease in the sheet stiffness.

In the presence of initial geometric imperfection, the plate is no longer a sheet and becomes three-dimensional. Therefore, in this case, "Eq. (4)" along with geometric imperfection-function is used. Although the imperfection function can exist in various forms, to study the amplitude, frequency and defect location parametrically, the initial geometric imperfection is represented as a three-dimensional surface as [35]:

$$w^i(x,y) = \xi\, h\, sech\left(\frac{\delta_1(x-x_c)}{a}\right)\cos\left(\frac{\mu_1\pi(x-x_c)}{a}\right) \operatorname{sech}\left(\frac{\delta_2(y-y_c)}{b}\right)\cos\left(\frac{\mu_2\pi(y-y_c)}{b}\right) \quad (40)$$

Where, ξ is the amplitude to thickness ratio, (x_c, y_c) is the position of the bulge maximum amplitude, (μ_1, μ_2) are imperfection half wave numbers in the x and y directions, respectively and (δ_1, δ_2) determine the localize degree of imperfection. In "Eq. (41)", hyperbolic functions determine the extension of the bulge, and trigonometric functions generate bulges with a maximum value in (x_c, y_c). Therefore, they create a wide range of initial geometric imperfection modes [35]. Two of these imperfections are shown in "Fig. 4".

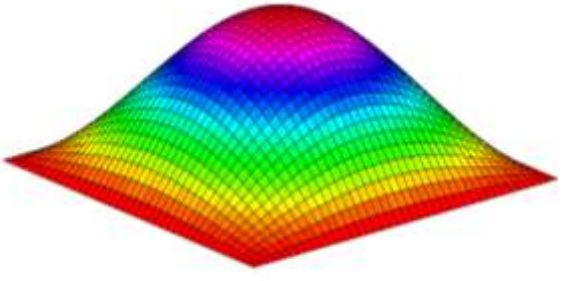

(a): Sine type: $\delta_1 = \delta_2 = 0,\ \mu_1 = \mu_2 = 1,\ \frac{x_c}{a} = \frac{y_c}{b} = 0.5$

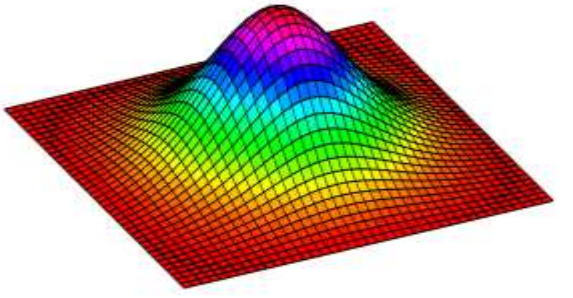

(b): L1 type: $\delta_1 = \delta_2 = 5,\ \mu_1 = \mu_2 = 1,\ \frac{x_c}{a} = \frac{y_c}{b} = 0.5$

Fig. 4 Sinusoidal and L1 type imperfection modes.

Fig. 5 shows variations of the imperfection sensitivity with imperfection amplitude (ξ) for a square SLGS with a Poisson ratio of 0.16. Imperfection sensitivity is defined as $S = \left|\frac{\omega^* - \bar{\omega}}{\bar{\omega}}\right| \times 100$, where $\bar{\omega}, \omega^*$, are the fundamental frequencies for perfect and imperfect SLGS, respectively. The sinusoidal imperfection type and SSSS boundary condition are considered here. As shown, the imperfection sensitivity increases with an increase in imperfection amplitude, since the stiffness and consequently the natural frequency of the plate increases. If the bulge maximum amplitude value approaches the plate thickness $(\xi = 1)$, then the natural frequency will reach twice the natural frequency of the perfect SLGS. Also, a greater thickness to side ratio gives a higher imperfection sensitivity. The amount of this increase is more visible for larger imperfection amplitudes.

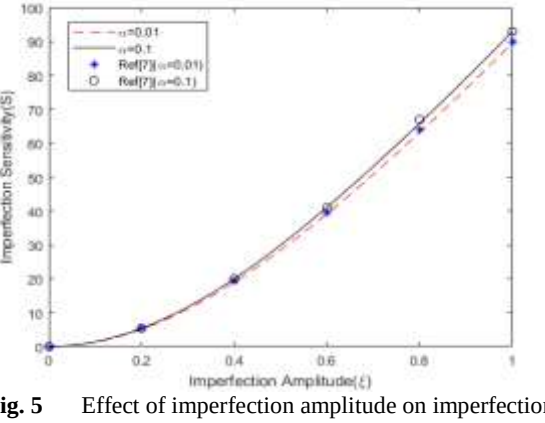

Fig. 5 Effect of imperfection amplitude on imperfection sensitivity for local square SLGS.

The variations of imperfection sensitivity for geometrically imperfect square SLGS with imperfection amplitude 'ξ' and the nonlocal parameter are depicted in "Fig. 6".

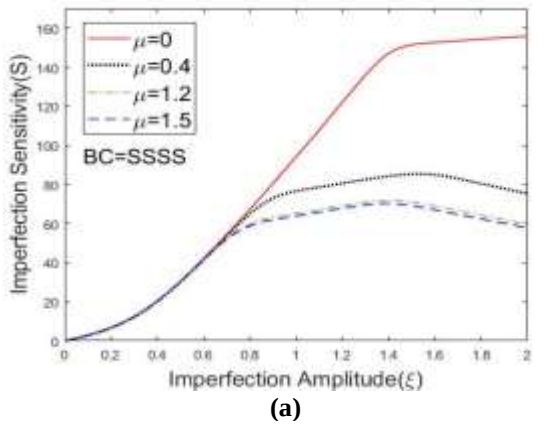

(a)

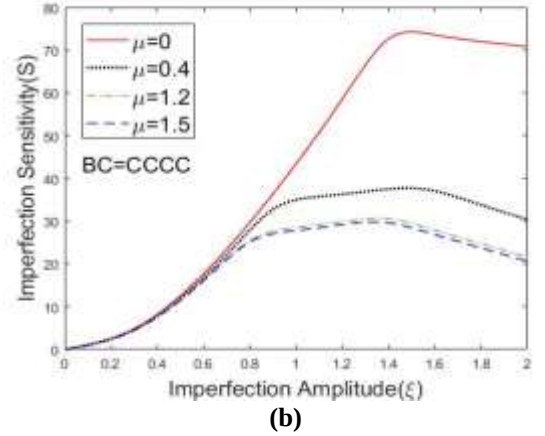

(b)

Fig. 6 Effect of imperfection amplitude on imperfection sensitivity for square SLGS (a=2 nm).

The sinusoidal imperfection type with a=2 nm is considered. In the SSSS boundary condition, for ξ<0.7, the imperfection sensitivity is independent of the nonlocal parameter. In this state, classical continuum and nonlocal theories give the same results. For higher imperfection amplitude, imperfection sensitivity decreases with increasing nonlocal parameter. For large imperfection amplitude (ξ>1.4), the imperfection sensitivity for nonlocal SLGS decreases. In local plates, with increasing d, the stiffness of the sheet and consequently the natural frequency always increases. In nonlocal sheets, with increasing ξ, the sheet stiffness as well as the natural frequency increase. But for larger ξ, the stiffness-softening phenomenon occurs in the sheet and the natural frequency of the sheet begins to decrease again. Also, the imperfection sensitivity for the large nonlocal parameter is less affected by the imperfection amplitude, while at lower nonlocal parameters, especially for the local plate, its effect is more visible. In the CCCC boundary condition, the variation of imperfection sensitivity is somewhat similar to SSSS, but it depends on the nonlocal parameter over a wider range of ξ and is independent of this parameter for ξ<0.3. Also, imperfection sensitivity in SLGS with clamped edges is lower than simply-supported edges. In other words, the geometric imperfection has less effect on the natural frequency of the clamped geometrically imperfect SLGS.

The effects of the imperfection extension parameter (δ) on imperfection sensitivity for SSSS and CCCC boundary conditions are shown in "Fig. 7". The results are depicted for several imperfection amplitudes ξ. As shown for the SSSS boundary condition, an increase in δ, which indicates a greater concentration of imperfection at the center of the nanoplate, decreases the imperfection sensitivity while decreasing δ and approaching to sinusoidal type, the imperfection sensitivity increases. When δ tends to large values, the imperfection sensitivity converges to a constant value for all ξ. For the CCCC boundary condition, as δ increases, the imperfection sensitivity increases first and then starts decreasing, so that the maximum value of imperfection sensitivity for all ξ occurs near δ=3.

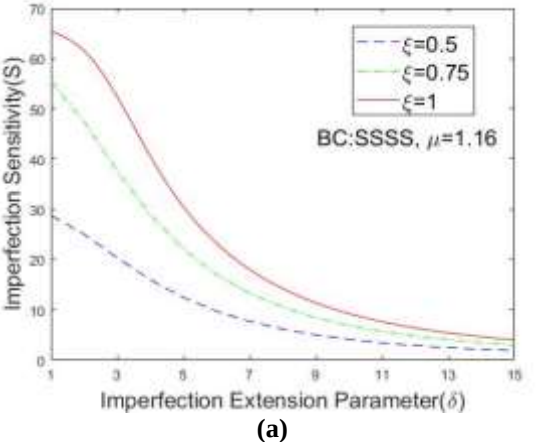

(a)

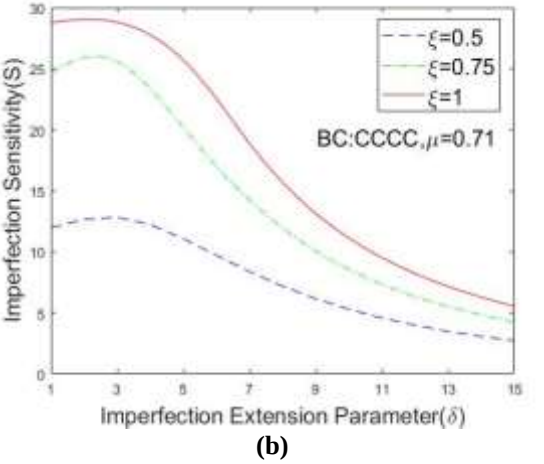

(b)

Fig. 7 Effect of imperfection extension parameter on imperfection sensitivity of square SLGS (a=2 nm).

Variations of frequency parameter (for geometrically imperfect SLGS) with imperfection amplitude and a/h

ratio, for both clamped and simply supported boundary conditions, are shown in "Fig. 8".

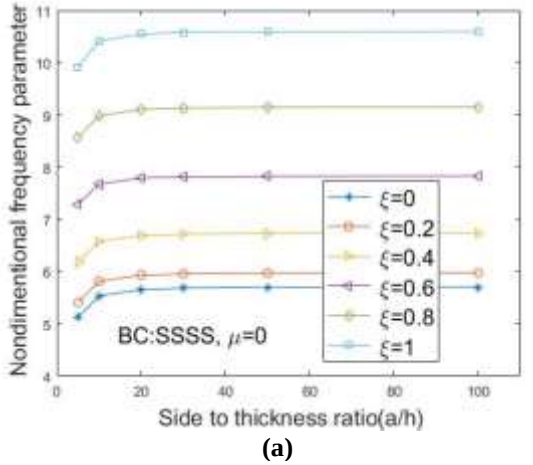

(a)

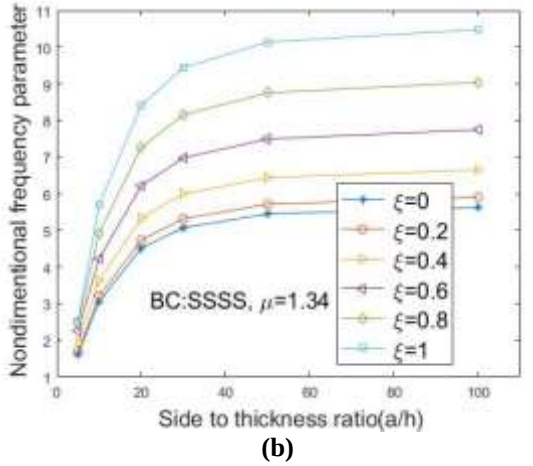

(b)

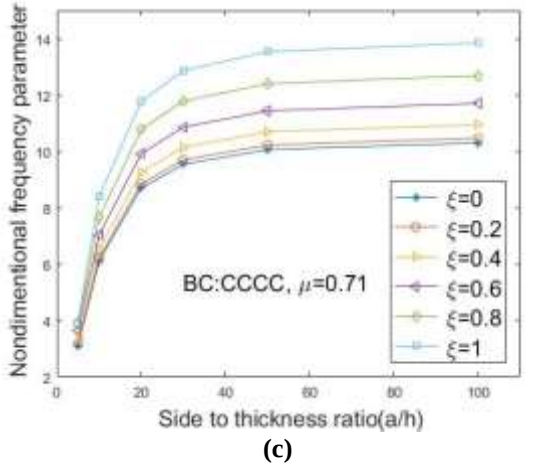

(c)

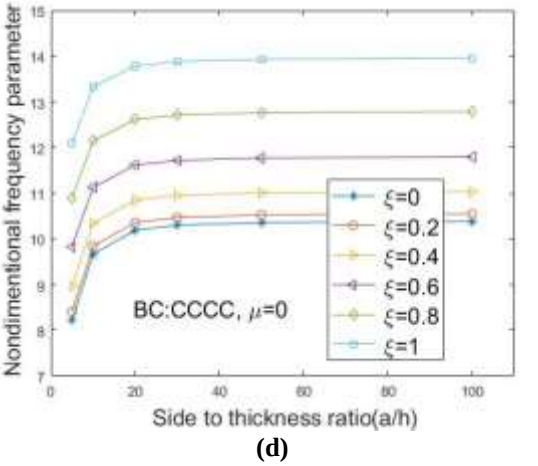

(d)

Fig. 8 The variation of frequency parameter of square SLGS with side to thickness ratio.

Both local $\mu = 0$ and nonlocal plates $(\mu \neq 0)$ are considered. The non-dimensional frequency parameter is considered as $\hat{\omega}=\omega\left(a^2/h\right)\sqrt{\rho(1-\nu^2)/E}$. It is observed that for both SSSS and CCCC boundary conditions, the frequency parameter for each ξ increases first with increasing side to thickness ratio and then converges to a constant value. Also, the frequency parameter increases with increasing ξ for all side to thickness ratios. The change in the frequency parameter between ξ=0 and ξ =1, for the SSSS boundary condition, is greater than that for the CCCC boundary condition. Therefore, it can be seen that the CCCC boundary condition reduces the effects of the geometric imperfection on the frequency parameter. Also, it can be seen that for the same boundary condition, the frequency parameter value in the non-local plate is less than that for the local plate. Another important point is that the non-local parameter at lower *a/h* has a greater effect on the frequency parameter. In other words, the geometric imperfection has a more significant effect on thick plates.

The effect of aspect ratio on the frequency parameter for nonlocal SLGS, for several imperfection amplitudes, is shown in "Fig. 9" for CCCC and SSSS boundary conditions. As it can be seen, the frequency parameter value decreases with increasing the aspect ratio. Also, the change in the frequency parameter between ξ=0 and ξ=1 decreases with increasing the aspect ratio. In other words, decreasing the aspect ratio results in greater effect of geometric imperfection on the non-dimensional frequency parameter.

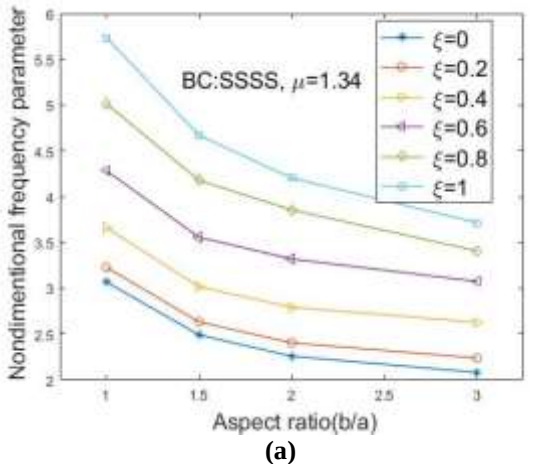

(a)

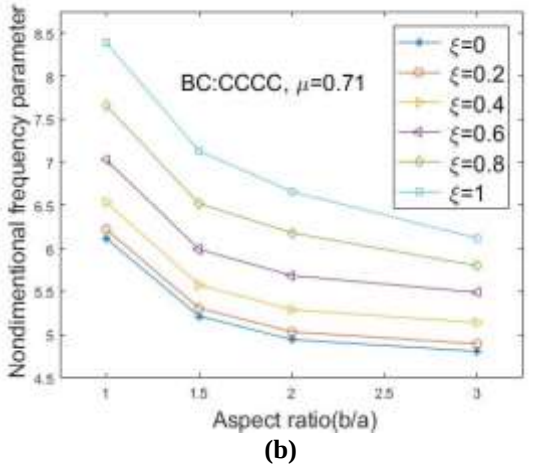

(b)

Fig. 9 Effect of aspect ratio on nondimensional frequency parameter of nonlocal SLGS (a/h=10).

As results show, the natural frequency of geometrically imperfect graphene sheets is significantly influenced by the nonlocal parameter. Therefore, it is necessary to use the appropriate value for this parameter. Ansari et al. [36] obtained the nonlocal parameter for pristine SLGS for simply supported and clamped boundary conditions. They proposed 1.41 (SSSS) and 0.87 (CCCC) for zigzag and 1.34 (SSSS) and 0.74 (CCCC) for armchair SLGS. Jalali et al. [4] compared the fundamental frequency for the pristine SLGS obtained from the continuum approach with that derived from the molecular dynamics method to find the appropriate nonlocal parameter and then used this parameter to analyze the geometrically imperfect SLGS.

In the present study, to find the appropriate nonlocal parameter value for geometrically imperfect SLGS, the fundamental frequencies of a pristine and localized imperfect ($\delta_1=\delta_2=5$, $\xi=1$) SLGS are investigated and shown in Table 4. The errors relative to molecular dynamics (MD) results reported by Jalali et al. [4] are also shown in the table. At $\mu=1.34$, the error for both pristine and localized SLGS are acceptable and this value for the nonlocal parameter can be used to analyze imperfect SLGS.

Table 4 Fundamental frequencies (THZ) for pristine and localized imperfect SLGS (a=2 nm, SSSS)

		Imperfection	
μ	Theory	Pristine	L1 Type
0	Present Study	1.580	2.142
	Jalali [4]	1.510	2.068
1.16	Present Study	0.609(4%)	0.794(7%)
	Jalali [4]	0.584(0%)	0.784(6%)
1.27	Present Study	0.584(0%)	0.764(3%)
1.34	Present Study	0.573(2%)	0.746(1%)
1.41	Present Study	0.560(4%)	0.729(1%)
	MD Jalali [4]	0.584	0.740

"Table 5" presents the fundamental frequencies for sinusoidal and localized imperfect SLGS for the case of simply supported and clamped boundary conditions.

Table 5 Fundamental frequencies (THZ) for SLGS with sinusoidal (δ=0) and localized (δ=5) imperfection (a=2 nm)

			μ			
δ	B.C	ξ	0	1.16	1.34	1.41
0	SSSS	0.7	2.440	0.930	0.874	0.855
		1	3.069	1.007	0.941	0.919
		1.25	3.612	1.038	0.970	0.947
		1.5	3.965	1.044	0.974	0.950
	CCCC	0.7	3.295	1.121	1.050	1.026
		1	3.830	1.191	1.112	1.085
		1.25	4.330	1.207	1.128	1.101
		1.5	4.643	1.200	1.119	1.092
5	SSSS	0.7	1.930	0.733	0.688	0.673
		1	2.142	0.795	0.746	0.729
		1.25	2.302	0.835	0.784	0.766
		1.5	2.446	0.868	0.814	0.795
	CCCC	0.7	3.108	1.097	1.029	1.005
		1	3.391	1.166	1.088	1.062
		1.25	3.605	1.165	1.087	1.061
		1.5	3.796	1.158	1.080	1.054

5 CONCLUSIONS

The size-dependent free vibration analysis and imperfection sensitivity for an imperfect SLGS via NURBS-based IGA, together with the quasi-3D deformation theory, has been examined. The initial geometric imperfection was modeled by inserting an analytical function in the governing Equations. Results show an excellent frequencies comparison for thin SLGS and different frequency values for thick SLGS.

The natural frequencies derived for clamped plates are less sensitive to geometric imperfection than simply supported plates. As the nonlocal parameter increases, the stiffness of the sheet and consequently the natural frequency decreases. The imperfection sensitivity for small values of imperfection amplitude is almost independent of the nonlocal parameter, while for larger values, it reduces by increasing the nonlocal parameter. For a large nonlocal parameter, changes in imperfection amplitude have an insignificant effect on imperfection sensitivity, whereas, for a small nonlocal parameter, imperfection sensitivity is susceptible to imperfection amplitude variations. By increasing the value of the imperfection extension parameter δ, the imperfection sensitivity decreases and converges to a constant value for all imperfection amplitudes. Frequencies for perfect and imperfect SLGS for different nonlocal parameters were extracted, and by comparing with the existing MD analysis, an appropriate and best fit nonlocal parameter value is found.

REFERENCES

[1] Terrones, M., Botello-Méndez, A. R., and Campos-Delgado, J, et al., Graphene and Graphite Nano Ribbons: Morphology, Properties, Synthesis, Defects and Applications, Nano Today, Vol. 5, 2010, pp. 351-372.

[2] Hierold, Ch., Jungen, A., Stampfer, C. H., and Helbling, T., Nano Electromechanical Sensors Based on Carbon Nanotubes, Sensors and Actuators A, Vol. 136, 2007, pp. 51-61.

[3] Wang, C. G., Lan, L., Liu, Y. P., and Tan, H. F., Defect-Guided Wrinkling in Graphene, Computational Materials Science, Vol. 77, 2013, pp. 250–253.

[4] Jalali, S. K., Pugno, N. M., and Jomehzadeh, E., Influence of Out-Of-Plane Defects on Vibration Analysis of Graphene Sheets: molecular and Continuum Approaches, Superlattices and Microstructures, Vol. 91, 2016, pp. 331-344.

[5] Lehtinen, O., Kurasch, S., Krasheninnikov, A. V., and Kaiser, U., Atomic Scale Study of The Life Cycle of a Dislocation in Graphene from Birth to Annihilation, Nat Commun, Vol. 4, 2013, 2098.

[6] Robertson, A. W., Allen, C. S., Wu, Y. A., He, K., Olivier, J., Neethling, J., Kirkland, A. I., and Warner, J. H., Spatial Control of Defect Creation in Graphene at The Nanoscale, Nat Commun, Vol. 3, 2012, 1144.

[7] Berthe, M., Yoshida, S., Ebine, Y., Kanazawa, K., Okada, A., Taninaka A., and et al, Reversible Defect Engineering of Single-Walled Carbon Nanotubes Using Scanning Tunneling Microscopy, Nano Lett, Vol. 7, 2007, pp. 3623–3627.

[8] Suleimani, A., Naei, M. H., and Mashhadi, M. M., Nonlocal Post Buckling Analysis of Graphene Sheets with Initial Imperfection Based on First Order Shear Deformation Theory, Results in Physics, Vol. 7, 2017, pp. 1299-1307.

[9] Jomehzadeh, E., Afshar, M. K., Galiotis, C., Shi, X., and Pugno, M. N., Nonlinear Softening and Hardening Nonlocal Bending Stiffness of An Initially Curved Monolayer Graphene, Compos Part B: Eng, Vol. 56, 2017, pp. 123-131.

[10] Eringen, A. C., Nonlocal Continuum Field Theories, Springer, NewYork. 2002.

[11] Sarrami-Foroushani, S., Azhari M., Nonlocal Buckling and Vibration Analysis of Thick Rectangular Nanoplates Using Finite Strip Method Based on Refined Plate Theory, Acta Mechanica, Vol. 227, 2016, pp. 721-742.

[12] Malekzadeh, P., Shojaee, M., Free Vibration of Nanoplates Based on A Nonlocal Two-Variable Refined Plate Theory, Compos. Struct, Vol. 95, 2013, pp. 443–452.

[13] Arash, B., Wang, Q., A Review on The Application of Nonlocal Elastic Models in Modeling of Carbon Nanotubes and Graphenes, Comp Mater Sci, Vol. 51, 2012, pp. 303–313.

[14] Bayati Chaleshtori, B., Hajiahmad, A., and Mohtasebi, S. S., Vibration Analysis of Rectangular Kirchhoff Nano-Plate using Modified Couple Stress Theory and Navier Solution Method, Int J of Advanced Design and Manufacturing Technology, Vol. 14, No. 2, 2021, pp. 85–92.

[15] Nourbakhsh, S. H., Botshekanan Dehkordi, M., and Atrian, A., Free Vibration Analysis of Nanoplates using Differential Transformation Method, Int J of Advanced Design and Manufacturing Technology, Vol. 10, No. 1, 2017, pp. 39-49.

[16] Thai, C. H., Ferreira A. J. M., and Phung-Van, P., Free Vibration Analysis of Functionally Graded Anisotropic Microplates Using Modified Strain Gradient Theory, Engineering Analysis with Boundary Elements, Vol. 117, 2020, pp. 284–298

[17] Senthilnathan, N. R., Lim, S. P., Lee, K. H., and Chow, S. T., Buckling of Shear-Deformable Plates, AIAA J, Vol. 25, 1987, pp. 1268–1271.

[18] Narendar, S., Buckling Analysis of Micro-/Nano-Scale Plates Based on Two-Variable Refined Plate Theory Incorporating Nonlocal Scale Effects, Compos, Struct, Vol. 93, 2011, pp. 3093–3103.

[19] Shimpi, R. P., Refined Plate Theory and Its Variants, AIAA J, Vol. 40, 2002, pp. 137–146.

[20] Nguyen, N. T., Hui, D., Lee, J., and Nguyen-Xuan, H., An Efficient Computational Approach for Size-Dependent Analysis of Functionally Graded Nanoplates, Comput. Methods Appl. Mech. Engrg, Vol. 297, 2015, pp. 191–218.

[21] Zenkour, A. M., Bending Analysis of Functionally Graded Sandwich Plates Using a Simple Four Unknown Shear and Normal Deformations Theory, J. Sandwich Struct. Mater, Vol. 15, 2013, pp. 629–656.

[22] Zenkour, A. M., A Simple Four-Unknown Refined Theory for Bending Analysis of Functionally Graded Plates, Appl. Math. Model, Vol. 37, 2013, pp. 9041–9051.

[23] Nguyen, H. X., Nguyen, T. N., Abdel-Wahab, M., Bordas, S. P. A., Nguyen-Xuan, H., and Vo, T. P., A Refined Quasi-3D Isogeometric Analysis for Functionally Graded Microplates Based on The Modified Couple Stress Theory, Comput. Methods Appl. Mech. Engrg, Vol. 313, 2017, pp. 904–940.

[24] Gupta, A., Talha, M., An Assessment of a Non-Polynomial Based Higher Order Shear and Normal Deformation Theory for Vibration Response of Gradient Plates with Initial Geometric Imperfections, Composites Part B, Vol. 107, 2016, pp. 141-161.
[25] Van Do, V. N., Lee, C. H., Free Vibration Analysis of Fgm Plates with Complex Cutouts by Using Quasi-3d Isogeometric Approach, International Journal of Mechanical Sciences, Vol. 159, 2019, pp. 213–233
[26] Phung-Van, P., Ferreira, A. J. M., Nguyen-Xuan, H., and Wahab, M. A., An Isogeometric Approach for Size-Dependent Geometrically Nonlinear Transient Analysis of Functionally Graded Nanoplates, Composites Part B, Vol. 118, 2017, pp. 125-134.
[27] Hughes, T. J. R., Cottrell, J. A., and Bazilevs, Y., Isogeometricanalysis: CAD, Finite Elements, Nurbs, Exact Geometry and Mesh Refinement, Comput Methods Appl Mech Eng, Vol. 194, 2005, pp. 4135–4195.
[28] Fazeli, H., Adamian, A., and Hosseini‑Sianaki, A., Influence of Initial Geometric Imperfection on Static and Free Vibration Analyses of Porous Fg Nanoplate Using an Isogeometric Approach, Journal of the Brazilian Society of Mechanical Sciences and Engineering, Vol. 43, No. 4, 2021, pp. 200.
[29] Soldatos, K. P., A Transverse Shear Deformation Theory for Homogeneous Monoclinic Plates, Acta Mech, Vol. 94, 1992, pp. 195–220.
[30] Nguyen-Xuan, H., Thai, C. H., and Nguyen-Thoi, T., Isogeometric Finite Element Analysis of Composite Sandwich Plates Using a Higher Order Shear Deformation Theory, Composites Part B, Vol. 55, 2013, pp. 558–574.
[31] Nguyen-Xuan, H., Tran, L. V., Thai, C. H., Kulasegaram, S., and Bordas S., Isogeometric Analysis of Functionally Graded Plates Using a Refined Plate Theory, Composites Part B, Vol. 64, 2014, pp. 222–234.
[32] Thai, H. T., Kim, S. E., A Simple Quasi-3D Sinusoidal Shear Deformation Theory for Functionally Graded Plates, Composite Structures, Vol. 99, 2013, pp. 172–180.
[33] Auricchio, F., Da Veiga, L. B., Buffa, A., Lovadina, C., Reali, and A., Sangalli, G., A Fully Locking-Free Isogeometric Approach for Plane Linear Elasticity Problems: A Stream Function Formulation, Comput. Methods Appl. Mech. Engrg, Vol. 197, 2007, pp. 160–172.
[34] Sarrami-Foroushani, S., Azhari M., Nonlocal Vibration and Buckling Analysis of Single and Multi-Layered Graphene Sheets Using Finite Strip Method Including van Der Waals Effects, Phys. E Low Dimens. Syst. Nanostruct, Vol. 57, 2014, pp. 83–95.
[35] Gupta, A., Talha, M., Nonlinear Flexural and Vibration Response of Geometrically Imperfect Gradient Plates Using Hyperbolic Higher-Order Shear and Normal Deformation Theory, Composites Part B, Vol. 123, 2017, pp. 241-261.
[36] Ansari, R., Sahmani, S., and Arash B., Nonlocal Plate Model for Free Vibrations of Single-Layered Graphene Sheets, Physics Letters A, Vol. 375, 2010, pp. 53–62.